A genetically-encoded fluorescent biosensor for visualization of acetyl-CoA in live cells

Smith, Joseph J. [1]; Valentino, Taylor R.[1,2]; Ablicki, Austin H.[1]; Banerjee, Riddhidev[1]; Colligan, Adam R.[3]; Eckert, Debra M.[4]; Desjardins, Gabrielle A.[1]; Diehl, Katharine L. [1]*

[1]Department of Medicinal Chemistry, University of Utah

[2]Current affiliation: Buck Institute for Research on Aging

[3]ARC Tangents Analytics

[4]Department of Biochemistry, University of Utah School of Medicine

*correspondence to k.diehl@utah.edu

Abstract

Acetyl-coenzyme A is a central metabolite that participates in many cellular pathways. Evidence suggests that acetyl-CoA production and consumption are highly compartmentalized in mammalian cells. Yet methods to measure acetyl-CoA in living cells are lacking. In this work, we engineer an acetyl-CoA biosensor from the bacterial protein PanZ and circularly permuted green fluorescent protein (cpGFP). We biochemically characterize the sensor and demonstrate its selectivity for acetyl-CoA over other CoA species. We then deploy the biosensor in *E. coli* and HeLa cells to demonstrate its utility in living cells. In *E. coli*, we show that the biosensor enables detection of rapid changes in acetyl-CoA levels. In human cells, we show that the biosensor enables subcellular detection and reveals the compartmentalization of acetyl-CoA metabolism.

Introduction

Acetyl-coenzyme A (acetyl-CoA) is a core metabolite that serves central metabolic, catabolic, anabolic, and signaling functions.[1,2] It is perhaps best known as the intermediate that links glycolysis to the tricarboxylic acid (TCA) cycle. Acetyl-CoA in the cytoplasm is used as the building block for the synthesis of fatty acids and cholesterol, and nucleocytoplasmic acetyl-CoA is the acetyl donor in protein acetylation. In the mitochondria, pyruvate dehydrogenase complex (PDC) converts pyruvate to acetyl-CoA. Acetyl-CoA is also produced from the catabolism of fatty acids in the mitochondria and peroxisomes[3] and of branched chain amino acids (BCAAs) in the mitochondria.[4] In the nucleocytoplasm, ATP citrate lyase (ACLY) cleaves citrate to acetyl-CoA and oxaloacetate, while acyl-CoA synthetase short-chain family member 2 (ACSS2) condenses acetate and coenzyme A to generate acetyl-CoA.[5] PDC can also be present outside the mitochondria and contribute to the nucleocytoplasmic pool of acetyl-CoA.[6–8] Acetyl-CoA produced in the mitochondria (or peroxisome) utilizes the carnitine shuttle via carnitine acetyltransferase (CrAT) to translocate into the nucleocytoplasm.[3,9,10] Once the acetyl-carnitine is in the nucleus, carnitine octanoyl transferase (CrOT)[10] converts it back to acetyl-CoA. Acetyl-CoA metabolism is a potential therapeutic target in diseases including cancer,[11–13] metabolic disease,[12,14,15] and neurodegenerative disease.[16–18]

Moreover, acetyl-CoA metabolism in bacteria and yeast is of interest since it is the precursor to many valuable chemicals such as isoprenoids, polyketides, and 3-hydroxypropionate.[19–21] Microbial factories offer a sustainable alternative to fossil fuel-derived chemical production.[22–24] Efforts in the field of microbial engineering have focused on maximizing acetyl-CoA in bacteria and yeast to increase the production efficiency of valuable downstream molecules.[19–21] Genetic

reporters for malonyl-CoA[25–29] have been utilized in these efforts,[26,30–33] highlighting the utility of biosensors for enabling metabolic engineering.

Current methods to quantify acetyl-CoA from cells include enzyme-coupled assays (e.g., PicoProbe™ Acetyl-CoA assay) and mass spectrometry.[34–37] Due to the relatively low abundance and poor stability of acetyl-CoA, indirect methods of acetyl-CoA detection are often employed,[38] such as by the analysis of isotopically labeled fatty acids[39,40] or protein acetylation.[1,34,37,41] Recent advances in quantitating acetyl-CoA and other CoA species from cells by stable isotope labeling of essential nutrients in cell culture (SILEC) and mass spectrometry have achieved subcellular resolution via fractionation of cells and enabled the investigation of acetyl-CoA compartmentation.[34,35] Nevertheless, these methods, whether direct or indirect, are inherently destructive toward cells or tissues, and subcellular information is dependent on the fidelity of the fractionation technique employed.

Fluorescent biosensors represent a complementary approach for metabolite detection. These sensors are most commonly constructed from a naturally occurring metabolite binding protein and one or more fluorescent proteins (FPs). Biosensors exist for many cellular metabolites (e.g., for ATP, NAD^+, glucose, etc.) to enable real time detection in live cells,[42–44] but there are only a few examples of acyl-CoA biosensors. For live cell imaging, there is a semisynthetic, FRET-based biosensor for CoA,[45] a ratiometric biosensor for long-chain fatty acyl-CoA esters ("LACSer"),[46] and split luciferase-based biosensor for malonyl-CoA ("FapR-NLuc").[47] A BRET-based acetyl-CoA biosensor has been reported which can detect acetyl- and propionyl-CoA from cell lysates, but it was not demonstrated to be suitable for live cell imaging in its current form.[48] In this work, we engineered a genetically-encodable fluorescent biosensor for acetyl-CoA and demonstrated the sensor's utility in live cell detection of acetyl-CoA in *E. coli* and human cells.

Results

Biosensor engineering

We first selected an acetyl-CoA binding protein that we predicted would be amenable to forming a biosensor. We chose the protein PanZ (also known as PanM), which is an endogenous acetyl-CoA sensor that regulates pantothenate synthesis in *E. coli* and other related enterococcus species.[49–51] PanZ is a GNAT (GCN5-related N-acetyltransferase) domain-containing protein but was shown to lack acetyltransferase activity.[49–51] PanZ binds acetyl-CoA, and this bound state is competent to bind the zymogen PanD and its activated form, aspartate α-decarboxylase (ADC). A structure of the PanZ/acetyl-CoA/PanD complex (PDB: 5LS7) and other biochemical data[49–51] suggested that PanZ is a suitable basis for a fluorescent acetyl-CoA sensor. We tested the binding of purified PanZ to acetyl-CoA and CoA using surface plasmon resonance (SPR) and measured a 7-fold higher affinity for acetyl-CoA versus CoA (**Figure S1**). Based on these data, we concluded that PanZ was a promising starting point for our biosensor.

To engineer a fluorescent biosensor, we screened insertion sites of circularly permuted GFP (cpGFP) in loop regions of PanZ (**Figure 1a**). The variants ranged widely in terms of fluorescence intensity (**Figure S2a and S2b**). Considering the fold-change between the +/- acetyl-CoA conditions (**Figure 1b**) and the overall fluorescence intensity of each variant, we selected the R69-E70 insertion site as the best-performing from the panel. We next undertook a linker length screen based on this R69-E70 variant. The initial R69-E70 construct contained an AS linker on either side of the cpGFP (i.e., Nterm-PanZ(1-69)-AS-cpGFP-AS-PanZ(70-137)-Cterm). The linker combinations shown were tested (**Figure 1C**). The GA linker at both the N-terminus and C-

terminus of cpGFP was revealed to perform better than the original AS linker by about 2.5-fold in terms of responsivity (**Figure S2c**). We termed this version of the biosensor PancACe (pronounced "pancake"; for PanZ Acetyl-CoA sensor; **Figure 2A, S2d**). To attempt further optimization of PancACe, we undertook a linker composition screen (**Figure S2e**). To narrow down which variants to test biochemically, we performed molecular modeling and docking studies (**Figures S3 and S4**). However, none of the linker compositions we tested performed better than PancACe (i.e., GA). Notably, the EE linker variant is a "turn off" sensor. We also tested variants of PancACe in which cpGFP was replaced with yellow (cpYFP, "banana PancACe") or blue (cpBFP, "blueberry PancACe") fluorescent protein using the same GA linkers as PancACe (**Figure S4f**). Neither variant performed as well as PancACe, and so we proceeded with PancACe.

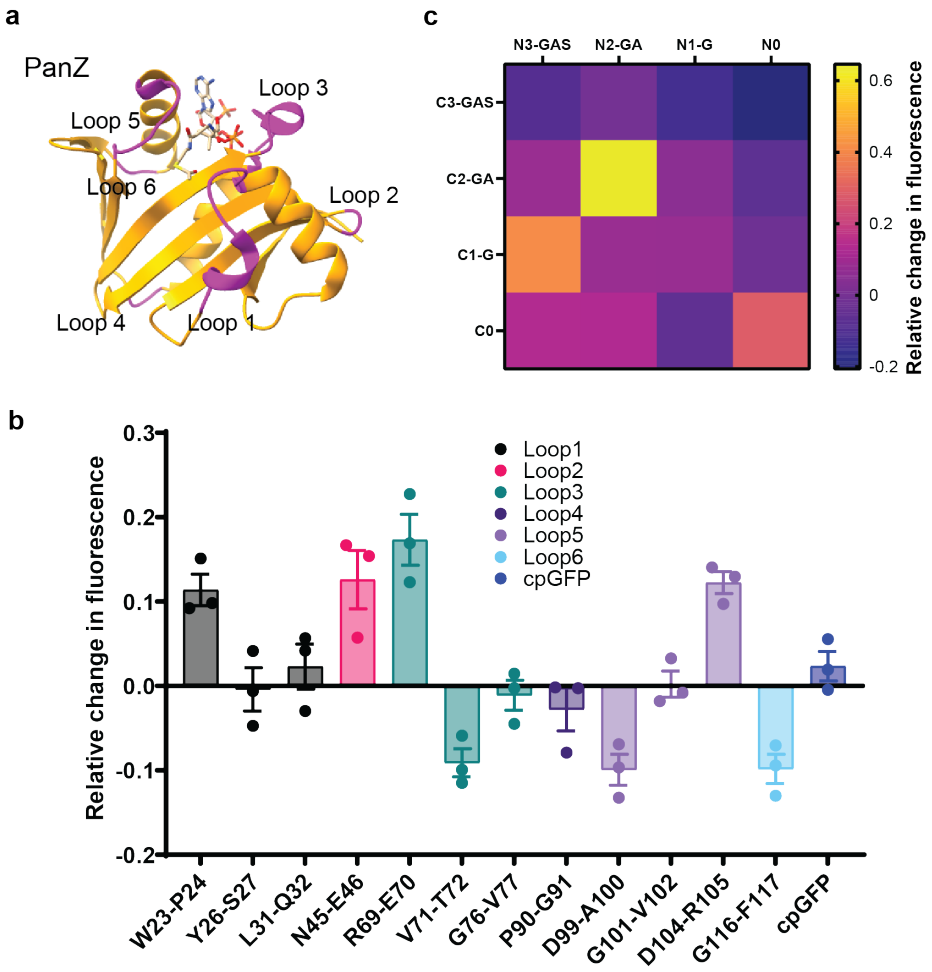

Figure 1. *Engineering of an acetyl-CoA biosensor from PanZ.* a) Crystal structure of PanZ (PDB: 5LS7) with the loops highlighted (magenta) into which cpGFP was inserted. b) Analysis of the loop insertion mutants. The data are displayed as relative fluorescence in the presence of 1 mM acetyl-CoA compared to in the absence of acetyl-CoA. n = 3. c) Analysis of the linker length variants (PanZ(1-69)-Ntermlinker-cpGFP-Ctermlinker-(70-137)PanZ fusion protein). The data are displayed as relative fluorescence in the presence of 1 mM acetyl-CoA compared to in the absence of acetyl-CoA. n = 1-3. For panels b-c, the data are displayed as the relative fluorescence: $(F_1-F_0)/F_0$). λ_{ex} = 485, λ_{em} = 514 nm, SEM shown for panel b.

Biochemical characterization of PancACe

We titrated PancACe or cpGFP with acetyl-CoA or CoA (**Figure 2b, S5a**). PancACe displays an increase in fluorescence upon binding to acetyl-CoA and has a maximum response of nearly 2-fold at saturating acetyl-CoA. This response range is comparable to other reported metabolite biosensors derived from a cpFP.[42,52,53] The affinity of PancACe for acetyl-CoA ($K_{D,app}$ = 274 ± 39 μM from fluorescence data, **Figure 2b**) is about 160-fold lower compared to PanZ (K_D = 1.7 ± 0.2 μM from SPR data, **Figure S1**). Since the R69-E70 insertion of cpGFP is very close to the acetyl-CoA binding site (**Figure 1a**, loop 3), this effect is not surprising. Indeed, a molecular model of the sensor shows that the cpGFP insertion alters the acetyl-CoA binding site of the PanZ significantly (**Figure S3**). PancACe shows good selectivity for acetyl-CoA over CoA (**Figure 2b**), which is consistent with our SPR binding data for PanZ (**Figure S1**). Even though the PancACe-CoA data cannot be fitted to obtain a $K_{D,app}$ since saturation was not achieved, interpolation between the PancACe-AcCoA and -CoA data indicates that 10 mM CoA is required to elicit the same sensor response as 100 μM acetyl-CoA. We further tested the selectivity of PancACe for short-chain acyl-CoAs (**Figure 2c**). The only other acyl-CoA that was recognized by the sensor was propionyl-CoA. Based on this single concentration experiment, the affinity of PancACe for propionyl-CoA is lower than for acetyl-CoA. A propionyl-CoA titration confirmed this apparent affinity difference (**Figure 2d**). Since saturation was not achieved up to 10 mM propionyl-CoA, we assumed that the same maximal sensor response would be achieved for propionyl-CoA as for acetyl-CoA. Based on this assumption, we fit the data and estimated a $K_{D,app}$ = 626 ± 75 uM for propionyl-CoA, a 2.3-fold lower affinity compared to acetyl-CoA. In most circumstances, there is likely much more acetyl-CoA in cells than propionyl-CoA. However, there are reports of conditions in which propionyl-CoA and acetyl-CoA concentrations are comparable such as in the nucleus.[34]

Since fluorescent proteins display pH sensitivity,[54,55] we measured the fluorescence of PancACe and cpGFP over pH 6.5-8 (**Figure S6**) and observed similar behavior as has been reported previously for an NAD^+ biosensor derived from cpVenus (cpV).[42] Since the pH sensitivity of PancACe and cpGFP are similar, cpGFP can be used in cells as a control for pH as a confounding influence on the PancACe signal. Finally, we sought to determine if we could use the same internal control that was used with the cpV-derived NAD^+ biosensor.[42] That group observed that a second excitation wavelength (λ_{ex} = 405 nm, λ_{em} = 520 nm) of cpV was largely invariant to the presence of NAD^+ and used this wavelength as an internal control for the amount of sensor present in their cell-based assays. PancACe and cpGFP also have this 405 nm excitation peak that is largely invariant to acetyl-CoA (**Figure S5b**) which we used for normalization in live cell experiments.

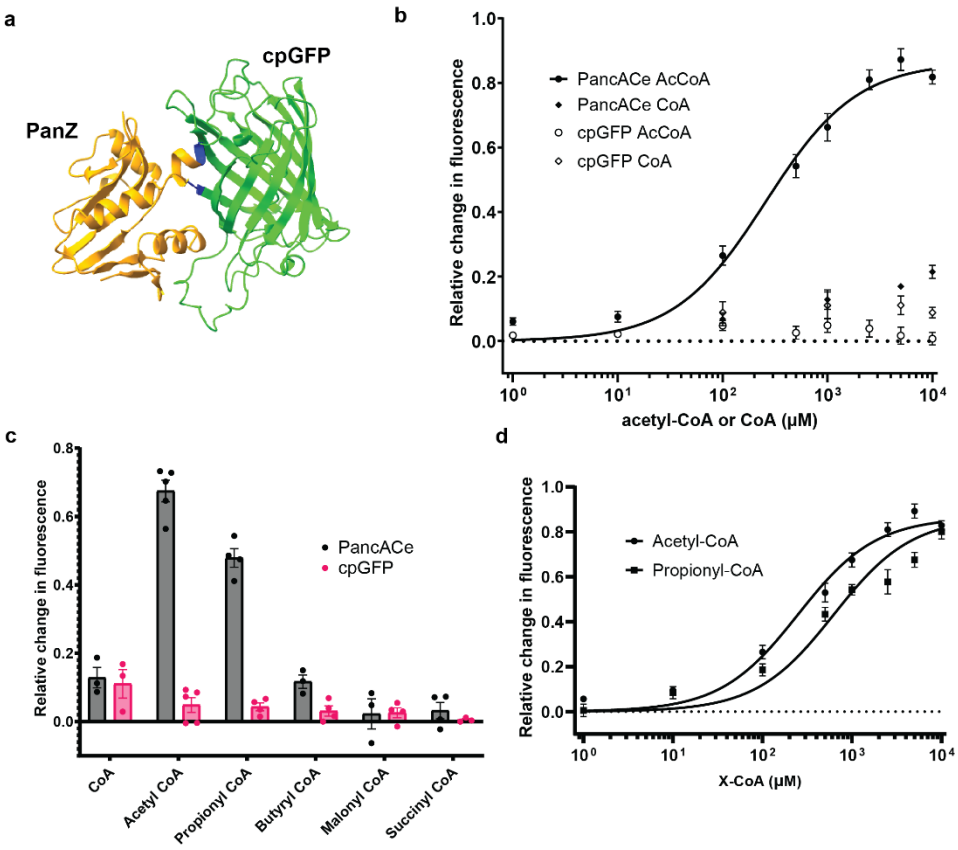

Figure 2. *Characterization of the biosensor PancACe.* a) Model of PancACe derived from PDB 5LS7 and 3O77. b) Titration of PancACe or cpGFP with acetyl-CoA or CoA. The PancACe + acetyl-CoA data were fitted to a one-site binding model. c) Selectivity testing of PancACe. The data were displayed as relative fluorescence in the presence of 1 mM X-CoA compared to in the absence of X-CoA. d) Titration of PancACe with propionyl-CoA. The data from panel b for PancACe + acetyl-CoA are reproduced on this plot for comparison. The data were fitted to a one-site binding model. For panels b-d, the data were displayed as the relative fluorescence: $(F_1-F_0)/F_0$). λ_{ex} = 485, λ_{em} = 514 nm, n = 3-5, SEM shown.

Acetyl-CoA measurements in live E. coli

We next used PancACe to measure acetyl-CoA in live *E. coli*. We expressed either PancACe or cpGFP in *E. coli*, manipulated the nutrient status of the cells, and measured the fluorescence of the cells via flow cytometry or well plate reader. We measured λ_{ex} = 405 nm and 485 nm (both with λ_{em} = 514 nm) to normalize the data (F_{488}/F_{405}) to account for changes due to pH, protein expression, photobleaching, or other factors that might influence the fluorescence signal but are not indicative of acetyl-CoA.

We reasoned that depriving *E. coli* of glucose and other nutrients would lead to a decrease in acetyl-CoA levels over time compared to cells treated with glucose. Therefore, we incubated cells in phosphate-buffered saline (PBS) for 3 hours and used flow cytometry to measure the fluorescence of the cells. We normalized the signal from each deprived time point to the signal measured in the fed condition, $(F_{deprived}-F_{fed})/F_{fed}$ (**Figure S7a**). We used cpGFP-expressing cells that were treated identically to the PancACe-expressing cells as a control. After 2 h of nutrient deprivation, PancACe showed a decrease in its fluorescence response while the cpGFP signal remained invariant over the entire time course (**Figure S7a**). Next, we performed a refeeding

experiment in which cells were first incubated in PBS for 3 h and then were refed with 28 mM glucose for 30 min, 1 h, 2 h, or 3 h. In this experiment, we normalized the signal from each refed time point to the signal measured in the deprived condition, $(F_{refed}-F_{deprived})/F_{deprived}$ (**Figure S7b**). Within 15 min, PancACe displayed a significant increase in signal, suggesting that the cells recovered their intracellular acetyl-CoA levels rapidly upon refeeding with glucose.

Since the change happened quickly during refeeding, we switched to using a well plate reader to measure the fluorescence *in situ* so that we could take repeated measurements of a cell population in shorter increments. We used injectors to rapidly add a concentrated bolus of the glucose, minimizing the volume change. First, we took cells that had either been pre-starved (no glucose for 3 h) or fed (+ 28 mM glucose for 3 h). Both sets of cells received ammonium as a nitrogen source. After briefly measuring the baseline signal, we added either 28 mM glucose to the deprived cells or buffer without glucose to the fed cells (**Figure 3a, S8**). Only the PancACe-expressing, starved cells that were refed with glucose showed a sharp increase in signal, and this occurred within about 5 min of feeding. Indeed, *E. coli* are able to rapidly exit dormancy, as they are accustomed to experiencing cycles of highly variable growth conditions.[56] Interestingly, acetyl-CoA appears to drop slightly from the initial peak before increasing again and reaching a stable level. We do not know what this behavior signifies, but our ability to detect it with PancACe highlights the power of this real-time approach.

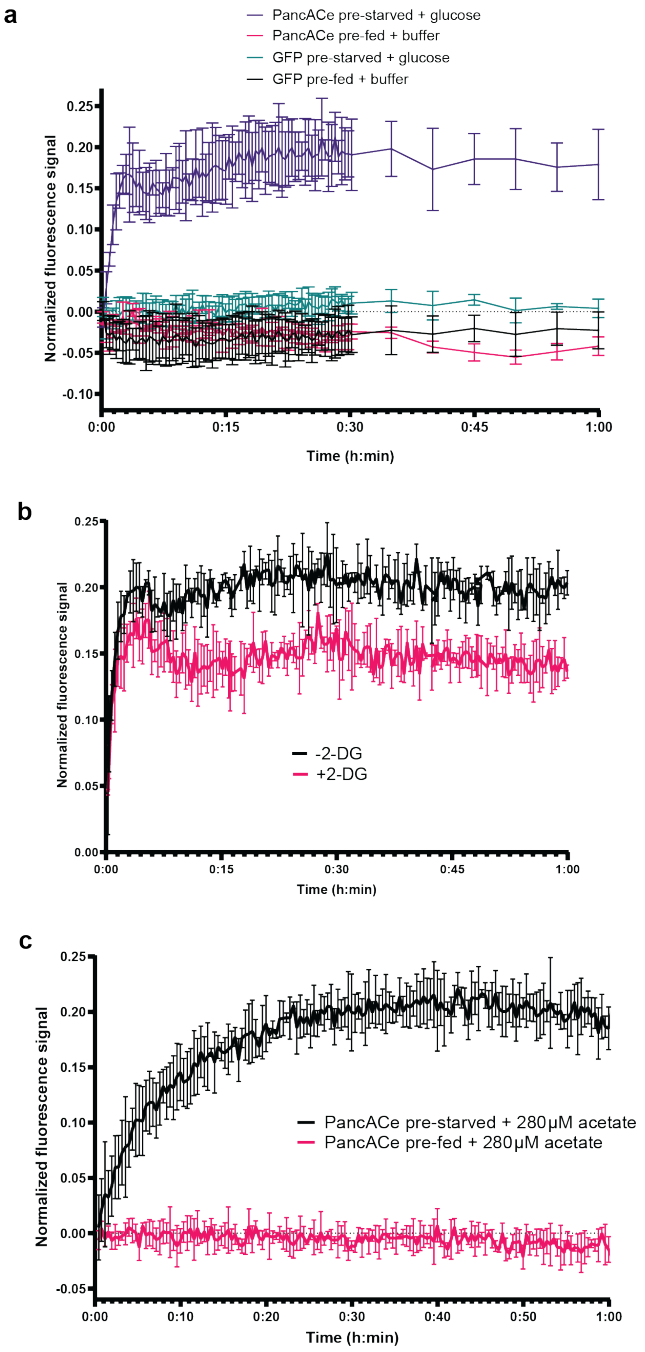

Figure 3. *Acetyl-CoA measurements in E. coli by PancACe.* a) Normalized fluorescence response of PancACe or cpGFP in *E. coli* to refeeding. The cells were either fed 28 mM glucose for 3 h prior ("pre-fed") or deprived of glucose for 3 h prior ("pre-starved"). At time 0:00, the cells were given either buffer alone ("+buffer") or 28 mM glucose ("+glucose"). b) Normalized fluorescence response of PancACe in *E. coli* to refeeding with or without 2-DG. The cells were deprived of glucose for 3 h prior either with or without 2-DG added. At time 0:00, the cells were given 28 mM glucose. c) Normalized fluorescence response of PancACe in *E. coli* to refeeding with acetate. The cells were either fed 28 mM glucose for 3 h prior ("pre-fed") or deprived of glucose for 3 h prior ("pre-starved"). At time 0:00, the cells were given 280 µM acetate. For panels a-c, the fluorescence was normalized by dividing F_{488}/F_{405} then $(F_1-F_0)/F_0$, where F_0 is defined by the fluorescence from each population of cells prior to time 0:00. λ_{ex} = 405,485, λ_{em} = 514 nm, n = 3

(technical replicates), SD shown. The additional experimental replicates (n = 3) are shown in **Figures S8-S10**.

Next, we treated cells with 2-deoxyglucose (2-DG), an inhibitor of glycolysis, prior to refeeding. Both groups of cells were deprived of glucose for 3 hours prior to refeeding, and one group also received 28 mM 2-DG during this period. Both groups exhibited an increase in PancACe signal upon refeeding with 28 mM glucose, but the cells treated with 2-DG demonstrated a suppressed increase over the refeeding time period (**Figure 3b, S9**).

Finally, we refed deprived or glucose-fed cells with acetate since acetate can be converted to acetyl-CoA via non-glycolytic pathways.[19] Acetate treatment led to a large increase in the deprived condition but no change in the glucose-fed condition (**Figure 3c, S10**). Interestingly, the increase occurred more gradually for acetate refeeding compared to glucose refeeding (**Figure 3a, S8**), supporting that these nutrients are used to make acetyl-CoA via different pathways. We also tested glucose or acetate refeeding on cells that had been fed glucose or acetate for an initial 3-hour period (**Figure S9d**). Only the cells that had initially been fed acetate and were refed with glucose showed a large increase in acetyl-CoA levels according to the sensor. This observation is consistent with glucose being the preferred energy source in these bacteria.[57,58]

Acetyl-CoA measurements in HeLa cells

We prepared HeLa cell lines stably expressing PancACe or cpGFP with a cytoplasmic ("cyto"), nuclear ("nuc"), or mitochondrial ("mito") localization tag (**Figure S11**).[42] To determine if the presence of the sensor alters free acetyl-CoA levels in the cells, we used the PicoProbe™ Assay and a histone acetylation immunoblot (**Figure S12**). The PicoProbe™ Assay showed no difference in free acetyl-CoA in the cells expressing cyto-cpGFP versus cyto-PancACe. The blots showed no difference in bulk histone acetylation in the cells expressing nuc-cpGFP versus nuc-PancACe. Together these results indicate that PancACe does not appreciably sequester acetyl-CoA in the cells. To measure acetyl-CoA levels in the cells with the biosensor, we used fluorescence microscopy to quantify the PancACe and cpGFP signals at excitation wavelengths of 405 and 488 nm (**Figure 4a, S11a**) for ratiometric analysis.

To perturb intracellular acetyl-CoA levels, we deprived the cells of glucose, complete serum (i.e., cells were given dialyzed fetal bovine serum, dFBS), glutamine, or combinations thereof for 16 h. We compared the sensor response to fed cells that were given complete media during the same period. The dFBS was used since normal FBS contains acetate, glucose, and other potential acetyl-CoA precursors[9] that dialysis is expected to reduce or eliminate. **Figure 4b-d** display the results for the three cellular compartments tested. Cytoplasmic acetyl-CoA levels were impacted by all of the deprivation conditions. Glucose or serum deprivation alone had a smaller impact than glutamine deprivation or deprivation combinations. The PicoProbe™ assay was used to measure free acetyl-CoA from cells that were glucose or glutamine deprived, and the assay results echoed the decreases reported by cyto-PancACe (**Figure S12b**).

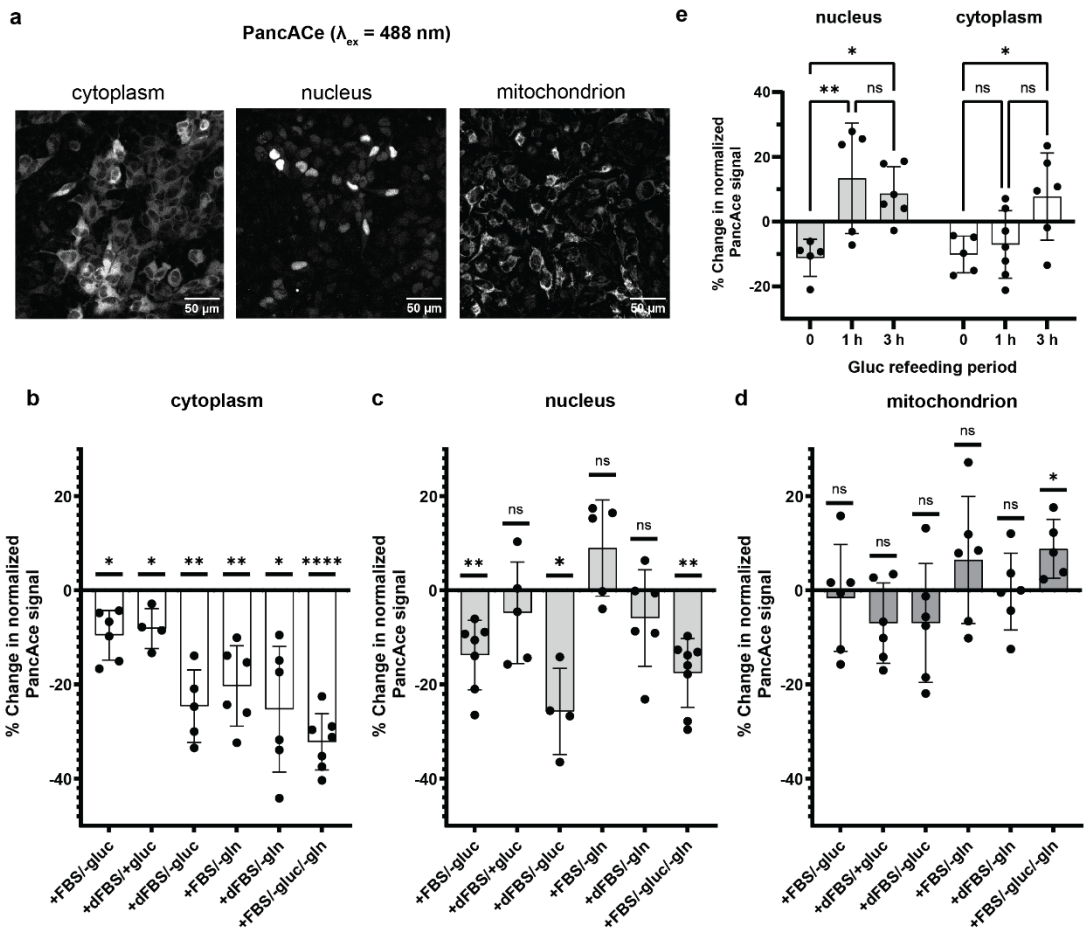

Figure 4. *Acetyl-CoA measurements by PancACe in nutrient-deprived HeLas*. a) Representative images for each PancACe cell line showing the subcellular localization to each compartment (λ_{ex} = 488). b-d) PancACe signal derived from images of HeLa cells expressing nuc-, cyto-, or mito-PancACe that were subjected to the indicated nutrient deprivation for 16 h. The data were collected and normalized as described in the Methods section. The data shown here are normalized to fed cells, n = 4-8 experimental replicates, SD shown. Two-tailed, paired t tests were performed on the data prior to normalization to the fed cells. The p values shown on the plot are for each condition compared to fed cells. e) PancACe signal derived from images of HeLa cells expressing nuc-PancACe or cyto-PancACe that were deprived of glucose for 16 h (time 0) and refed with 4.5 g/L glucose for 1 h or 3 h. The data were collected and normalized as described in the Methods section. The data shown here are normalized to fed cells. n = 4-7 experimental replicates, SD shown. Two-tailed, paired t tests were performed to compare 0, 1, or 3 h to fed cells prior to normalization to fed cells. Two-tailed, unpaired t test were performed to compare 1 and 3 h to 0 h. *p<0.05, **p<0.01, ****p<0.0001. All of the p values are shown in **Tables 1-2**.

In contrast, nuclear acetyl-CoA levels were sensitive to glucose deprivation but not glutamine or serum deprivation alone, although combined serum/glucose deprivation had a larger impact than glucose deprivation alone. Bulk histone acetylation data recapitulated the trends reported by nuc-PancACe (**Figure S13a-d**). In the mitochondria, only the elimination of both glucose and glutamine led to a significant change in acetyl-CoA levels. Interestingly, this condition resulted in an increase in acetyl-CoA compared to fed cells. This behavior could be due to the cells increasing β-oxidation to meet their energy needs in the absence of glucose and glutamine.[59]

Next, we tested the recovery of the cells after deprivation. The cells were glucose deprived for 16 h then refed with glucose for 1 h or 3 h (**Figure 4e**). Both cytoplasmic and nuclear acetyl-CoA levels fully recovered within 3 h of refeeding. At 1 h, there was more variability in the nucleus compared to the cytoplasm. Some of the nuclear experimental replicates showed an overcompensation effect at 1 h, suggesting that a surge of acetyl-CoA occurs in the nucleus upon refeeding. This effect was not observed in the cytoplasm at 1 h, indicating a steadier increase in acetyl-CoA upon refeeding in this compartment. When we looked at bulk histone acetylation levels under these same conditions (**Figure S14**), we observed that the levels were beginning to recover after 3 h, which is consistent with a lag between acetyl-CoA level rescue and acetyltransferase activity.

Since PancACe only has a 2.3-fold lower affinity for propionyl-CoA compared to acetyl-CoA, we wanted to evaluate its sensitivity to changes in cellular propionyl-CoA. Previous work showed that branched chain amino acid (BCAA) deprivation lowered nuclear propionyl-CoA levels but not nuclear acetyl-CoA levels.[34] In this prior study, the magnitudes of the cytoplasmic reduction in both acetyl- and propionyl-CoA levels were similar under BCAA restriction. We gave cells either complete media or media lacking the BCAAs valine and isoleucine for 24 h prior to imaging (**Figure S15a**). According to PancACe, nuclear acetyl-CoA levels did not change significantly, but cytoplasmic levels dropped to a similar extent as in glutamine or serum/glucose deprivation (**Figure 4b**). Histone acetylation blots showed no decrease in bulk histone acetylation in the BCAA-deprived cells (**Figure S15b,c**). These results are consistent with the prior study's findings and support that PancACe is reporting primarily on acetyl-CoA and not propionyl-CoA.

Acetyl-CoA is produced and consumed by different pathways in the cell in a compartmentalized fashion (**Figure 5a**). Thus, to measure compartment-specific changes in acetyl-CoA levels using PancACe, we knocked down a panel of proteins (**Figure S16**) that are involved in the production (ACLY, ACSS2, and Pyruvate dehydrogenase E1 component subunit alpha, PDHA), trafficking (CrAT), or consumption (p300 and acetyl-CoA carboxylase, ACC) of acetyl-CoA (**Figure 5b-d**). In the cytoplasm, we observed that the ACLY and ACSS2 knockdowns led to a decrease in acetyl-CoA levels. The CrAT knockdown showed a decreasing trend but was not statistically significant. In the nucleus, we observed that the ACSS2 and PDHA knockdowns decreased acetyl-CoA levels. The ACLY and CrAT knockdowns showed a decreasing trend but were not statistically significant. Knockdown of the acetyltransferase p300 had no statistically significant effect on acetyl-CoA levels in any of the compartments. The cytoplasm and mitochondria showed an accumulation of acetyl-CoA in the ACC knockdown, Knockdown of ACC is expected to reduce fatty acid synthesis and lead to accumulation of acetyl-CoA. We note that the variability in the nuc-PancACe data was too high to determine if the ACC knockdown was statistically significant, although it was trending as an increase. Other than accumulation of acetyl-CoA in the ACC knockdown, mitochondrial acetyl-CoA levels were unaffected by these perturbations. Based on previous cellular fractionation data, mitochondrial acetyl-CoA levels are relatively low compared to nucleocytoplasmic levels.[34] One possible explanation for this observation is that mitochondrial acetyl-CoA is converted rapidly into citrate (or acetyl-carnitine for export) rather than accumulating. Therefore, the changes in mitochondrial free acetyl-CoA may be relatively small under the knockdowns. Relatedly, PancACe may not be sensitive enough to detect small changes in an already low level of free acetyl-CoA in this compartment, especially decreases from the baseline.

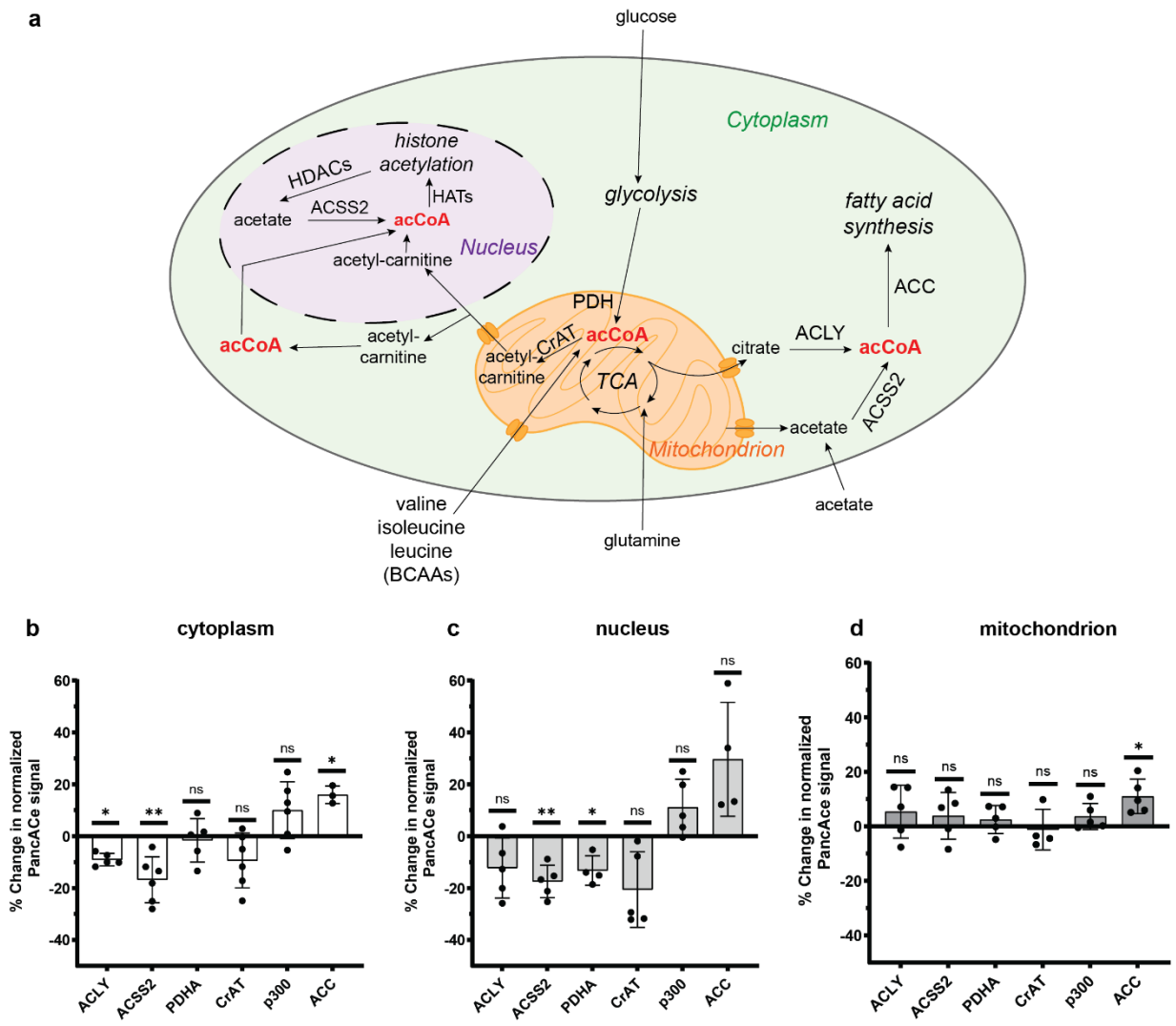

Figure 5. *Compartmentalization of acetyl-CoA in human cells*. a) Pathways of acetyl-CoA metabolism that we tested with PancACe in the HeLA cells. acCoA = acetyl-CoA, TCA = tricarboxylic acid cycle, ACLY = ATP-citrate lyase, ACSS2 = acetyl-CoA synthetase short chain 2, PDH = pyruvate dehydrogenase, CrAT = carnitine acetyltransferase, ACC = acetyl-CoA carboxylase, HATs = histone acetyltransferases, HDACs = histone deacetylases, BCAAs = branched-chain amino acids. b-d) PancACe signal derived from images of HeLa cells expressing nuc-, cyto-, or mito-PancACe that were subjected to the indicated siRNA knockdown for 48 h. The data were collected and normalized as described in the Methods section. The data shown here are normalized to non-targeted siRNA ("NT") cells, n = 3-6 experimental replicates, SD shown. Two-tailed, paired t tests were performed on the data prior to normalization to the NT cells. The p values shown on the plot are each condition compared to NT cells. *p<0.05, **p<0.01. All of the p values are shown in **Table 3**.

Discussion

We report herein a fluorescent biosensor for acetyl-CoA that we call "PancACe." PancACe consists of cpGFP embedded within the acetyl-CoA binding protein, PanZ. As the PanZ domain changes conformation from the unbound to the bound state, the intervening cpGFP is perturbed in its fluorescence emission, leading to an increase in cpGFP fluorescence in the bound state compared to the unbound state (i.e., a "turn on" sensor). Our data show that the insertion of the

cpGFP in PancACe leads to significant alteration of the acetyl-CoA binding site compared to PanZ alone. This change results in a large decrease in affinity for acetyl-CoA. Intracellular acetyl-CoA levels in *E. coli* are reported in the range of 20-600 μM,[60] while human cells are reported to be in the 1-30 μM range.[34,41] Based on these figures, PancACe's affinity for acetyl-CoA is suitable for use in *E. coli*. In human cells, PancACe is likely limited by its sensitivity, particularly in the mitochondria.[34] Nevertheless, we were able to detect changes in acetyl-CoA levels across all three compartments in human cells. We further demonstrated that the sensor is responding primarily to acetyl-CoA levels in human cells, suggesting suitable selectivity over propionyl-CoA. Future engineering efforts will focus on producing variants of PancACe with a range of affinities for acetyl-CoA. As is true of other cpFP-based biosensors, the linkers that connect the cpGFP to the PanZ binding domain play a crucial role in determining the responsivity (**Figure 1c**), and perhaps also the affinity, of the sensor. As indicated by our molecular modeling efforts, many challenges still exist with using a computational approach to aid in linker design, highlighting the need in the biosensor field for more refined methods for linker prediction and screening.

A potential application of PancACe is to aid in the metabolic engineering of bacteria or yeast for the production of biofuels or other valuable chemical products. Malonyl-CoA reporters have already been used in this way.[26,30,31,33] PancACe's affinity is well-matched to reported bacterial acetyl-CoA levels.[60] We show that the PancACe signal can be monitored in bulk bacterial cultures using a standard well plate reader. The real-time monitoring capability enables detection of rapid changes in acetyl-CoA levels. Alternatively, cells could be sorted by fluorescence to select for subpopulations based on their acetyl-CoA levels as part of a directed evolution workflow.

We further demonstrated that PancACe can be used to report on acetyl-CoA levels in live mammalian cells via fluorescence microscopy. Despite intracellular levels being on the low end of PancACe's dynamic range, we were able to detect changes in cytoplasmic and nuclear acetyl-CoA levels using ratiometric analysis (ex488/405 and PancACe/cpGFP). We were also able to detect increases in mitochondrial acetyl-CoA. Acetyl-CoA is produced from multiple pathways and precursor molecules, and many of these pathways can compensate for one another.[9,61] Nevertheless, our sensor was able to detect changes from only partial knockdowns of single proteins involved in acetyl-CoA metabolism. By targeting PancACe to different subcellular compartments, we can observe the compartmentalization of acetyl-CoA metabolism in these cells (**Figure 5a**). Our findings are consistent with the growing body of evidence that the nucleocytoplasm is not a single homogenous pool of acetyl-CoA[2,5,6,34,62–66] even though acetyl-CoA is small enough to pass freely through the nuclear pore.[5] We expect that PancACe and future iterations thereof will be very useful in measuring compartment-specific acetyl-CoA levels in different cell types and potentially in organisms as well.

Acknowledgements

This work was supported by the National Institutes of Health R35GM143080. G.D. was supported by the Undergraduate Research Opportunity Program (UROP) at the University of Utah. We acknowledge the Cell Imaging Core at the University of Utah for use of equipment (Leica SP8 Confocal Microscope) and thank Dr. Michael Bridge for his assistance. We also acknowledge the DNA/Peptide Synthesis, Flow Cytometry, and Drug Discovery Cores at the University of Utah. We acknowledge ChapGPT versions 3.5 and 4 (OpenAI) for assistance in writing the image processing script.

Author Contributions

J.J.S., T.R.V., and K.L.D. designed the experiments. J.J.S. performed the cloning, protein purification, biochemical assays with the sensors, and the *E. coli* assays. T.R.V. generated the stable cell lines and established the microscopy assay in the HeLa cells. A.H.A. performed the PicoProbe assay, some cloning and protein purification, and the linker composition experiments. R.B. performed the molecular modeling of PanZ and PancACe. A.R.C. wrote and employed the Python, Fiji macro, and SQLite scripting code for image data acquisition and initial processing of data to the well level. D.M.E. performed the surface plasmon resonance (SPR) assays. G.A.D. performed some cloning and protein purification and the YFP and BFP experiments. K.L.D. performed the immunoblot assays, the microscopy assays in the HeLa cells, and the analysis of the image data. J.J.S. and K.L.D. wrote the manuscript with input from all authors.

Conflicts of Interest

A United States patent with K.L.D. and J.J.S. as inventors has been filed on the technology described herein.

References

1. Shi, L. & Tu, B. P. Acetyl-CoA and the Regulation of Metabolism: Mechanisms and Consequences. *Curr. Opin. Cell Biol.* **33**, 125–131 (2015).

2. Pietrocola, F., Galluzzi, L., Bravo-San Pedro, J. M., Madeo, F. & Kroemer, G. Acetyl Coenzyme A: A Central Metabolite and Second Messenger. *Cell Metab.* **21**, 805–821 (2015).

3. Kuna, R. S. *et al.* Inter-organelle cross-talk supports acetyl-coenzyme A homeostasis and lipogenesis under metabolic stress. *Sci. Adv.* **9**, eadf0138 (2023).

4. Neinast, M., Murashige, D. & Arany, Z. Branched Chain Amino Acids. *Annu. Rev. Physiol.* **81**, 139–164 (2019).

5. Sivanand, S., Viney, I. & Wellen, K. E. Spatiotemporal Control of Acetyl-CoA Metabolism in Chromatin Regulation. *Trends Biochem. Sci.* **43**, 61–74 (2018).

6. Sutendra, G. *et al.* A Nuclear Pyruvate Dehydrogenase Complex Is Important for the Generation of Acetyl-CoA and Histone Acetylation. *Cell* **158**, 84–97 (2014).

7. Li, W. *et al.* Nuclear localization of mitochondrial TCA cycle enzymes modulates pluripotency via histone acetylation. *Nat. Commun.* **13**, 7414 (2022).

8. Zhang, J. *et al.* PARylated PDHE1α generates acetyl-CoA for local chromatin acetylation and DNA damage repair. *Nat. Struct. Mol. Biol.* 1–16 (2023) doi:10.1038/s41594-023-01107-3.

9. Izzo, L. T. *et al.* Acetylcarnitine shuttling links mitochondrial metabolism to histone acetylation and lipogenesis. *Sci. Adv.* **9**, eadf0115 (2023).

10. Hsu, J. *et al.* Carnitine octanoyltransferase is important for the assimilation of exogenous acetyl-L-carnitine into acetyl-CoA in mammalian cells. *J. Biol. Chem.* **299**, 102848 (2022).

11. Guertin, D. A. & Wellen, K. E. Acetyl-CoA metabolism in cancer. *Nat. Rev. Cancer* **23**, 156–172 (2023).

12. Wang, Y. *et al.* Acetyl-CoA Carboxylases and Diseases. *Front. Oncol.* **12**, (2022).

13. Ling, R. *et al.* Acetyl-CoA synthetase 2(ACSS2): a review with a focus on metabolism and tumor development. *Discov. Oncol.* **13**, 58 (2022).

14. Assante, G. *et al.* Acetyl-CoA metabolism drives epigenome change and contributes to carcinogenesis risk in fatty liver disease. *Genome Med.* **14**, 67 (2022).

15. Morrow, M. R. *et al.* Inhibition of ATP-citrate lyase improves NASH, liver fibrosis, and dyslipidemia. *Cell Metab.* **34**, 919-936.e8 (2022).

16. Lin, Y. *et al.* ACSS2-dependent histone acetylation improves cognition in mouse model of Alzheimer's disease. *Mol. Neurodegener.* **18**, 47 (2023).

17. Moiseenok, A. G. & Kanunnikova, N. P. Brain CoA and Acetyl CoA Metabolism in Mechanisms of Neurodegeneration. *Biochem. Biokhimiia* **88**, 466–480 (2023).

18. Jankowska-Kulawy, A., Klimaszewska-Łata, J., Gul-Hinc, S., Ronowska, A. & Szutowicz, A. Metabolic and Cellular Compartments of Acetyl-CoA in the Healthy and Diseased Brain. *Int. J. Mol. Sci.* **23**, 10073 (2022).

19. Zhang, S. *et al.* Metabolic engineering for efficient supply of acetyl-CoA from different carbon sources in Escherichia coli. *Microb. Cell Factories* **18**, 130 (2019).

20. Krivoruchko, A., Zhang, Y., Siewers, V., Chen, Y. & Nielsen, J. Microbial acetyl-CoA metabolism and metabolic engineering. *Metab. Eng.* **28**, 28–42 (2015).

21. Liu, W., Zhang, B. & Jiang, R. Improving acetyl-CoA biosynthesis in Saccharomyces cerevisiae via the overexpression of pantothenate kinase and PDH bypass. *Biotechnol. Biofuels* **10**, 41 (2017).

22. Gohil, N., Bhattacharjee, G. & Singh, V. An introduction to microbial cell factories for production of biomolecules. in *Microbial Cell Factories Engineering for Production of Biomolecules* (ed. Singh, V.) 1–19 (Academic Press, 2021). doi:10.1016/B978-0-12-821477-0.00021-0.

23. Cho, J., Kim, G., Eun, H., Moon, C., & Lee, S. Designing Microbial Cell Factories for the Production of Chemicals. *J. Am. Chem. Soc. Au* **2**, 1781–1799.

24. Lee, S. Y. *et al.* A comprehensive metabolic map for production of bio-based chemicals. *Nat. Catal.* **2**, 18–33 (2019).

25. Ellis, J. M. & Wolfgang, M. J. A genetically encoded metabolite sensor for malonyl-CoA. *Chem. Biol.* **19**, 1333–1339 (2012).

26. Johnson, A. O. *et al.* Design and application of genetically-encoded malonyl-CoA biosensors for metabolic engineering of microbial cell factories. *Metab. Eng.* **44**, 253–264 (2017).

27. He, S., Zhang, Z., Zhang, C. & Lu, W. Construction and Optimization of Malonyl-CoA Sensors in Saccharomyces cerevisiae by Combining Promoter Engineering Strategies. *Processes* **10**, 2660 (2022).

28. Xu, P. *et al.* Design and Kinetic Analysis of a Hybrid Promoter–Regulator System for Malonyl-CoA Sensing in Escherichia coli. *ACS Chem. Biol.* **9**, 451–458 (2013).

29. Kalkreuter, E. *et al.* Development of a genetically-encoded biosensor for detection of polyketide synthase extender units in Escherichia coli. *ACS Synth. Biol.* **8**, 1391–1400 (2019).

30. Yang, D. *et al.* Repurposing type III polyketide synthase as a malonyl-CoA biosensor for metabolic engineering in bacteria. *Proc. Natl. Acad. Sci. U. S. A.* **115**, 9835–9844 (2018).

31. Li, H., Chen, W., Jin, R., Jin, J.-M. & Tang, S.-Y. Biosensor-aided high-throughput screening of hyper-producing cells for malonyl-CoA-derived products. *Microb. Cell Factories* **16**, 187 (2017).

32. Qiu, C., Tao, H., Shen, Y., Qi, Q. & Hou, J. Dynamic-tuning yeast storage carbohydrate improves the production of acetyl-CoA-derived chemicals. *iScience* **26**, 105817 (2023).

33. Qui, C., Huang, M. Hou, Y., Tao, H., Zhao, J., Shen, Y., Bao, X., Qi, Q., Hou, J. Biosensor-Coupled In Vivo Mutagenesis and Omics Analysis Reveals Reduced Lysine and Arginine Synthesis To Improve Malonyl-Coenzyme A Flux in Saccharomyces cerevisiae. *mSystems* **7**, e0136621 (2022).

34. Trefely, S. *et al.* Quantitative subcellular acyl-CoA analysis reveals distinct nuclear metabolism and isoleucine-dependent histone propionylation. *Mol. Cell* **82**, 447-462.e6 (2022).

35. Trefely, S. *et al.* Subcellular metabolic pathway kinetics are revealed by correcting for artifactual post harvest metabolism. *Mol. Metab.* **30**, 61–71 (2019).

36. Soaita, I. *et al.* Dynamic protein deacetylation is a limited carbon source for acetyl-CoA–dependent metabolism. *J. Biol. Chem.* **299**, 104772 (2023).

37. Sidoli, S., Trefely, S., Garcia, B. A. & Carrer, A. Integrated Analysis of Acetyl-CoA and Histone Modification via Mass Spectrometry to Investigate Metabolically Driven Acetylation. in *Cancer Metabolism: Methods and Protocols* (ed. Haznadar, M.) 125–147 (Springer New York, 2019). doi:10.1007/978-1-4939-9027-6_9.

38. Wellen, K. E. & Snyder, N. W. Should we consider subcellular compartmentalization of metabolites, and if so, how do we measure them? *Curr. Opin. Clin. Nutr. Metab. Care* **22**, 347–354 (2019).

39. Kamphorst, J. J., Chung, M. K., Fan, J. & Rabinowitz, J. D. Quantitative analysis of acetyl-CoA production in hypoxic cancer cells reveals substantial contribution from acetate. *Cancer Metab.* **2**, 23 (2014).

40. Tumanov, S., Bulusu, V. & Kamphorst, J. J. Analysis of Fatty Acid Metabolism Using Stable Isotope Tracers and Mass Spectrometry. *Methods Enzymol.* **561**, 197–217 (2015).

41. Simithy, J. *et al.* Characterization of histone acylations links chromatin modifications with metabolism. *Nat. Commun.* **8**, 1141–1153 (2017).

42. Cambronne, X. A. *et al.* Biosensor reveals multiple sources for mitochondrial NAD+. *Science* **352**, 1474 LP – 1477 (2016).

43. White, D. & Yang, Q. Genetically Encoded ATP Biosensors for Direct Monitoring of Cellular ATP Dynamics. *Cells* **11**, 1920 (2022).

44. Leopold, A. V., Shcherbakova, D. M. & Verkhusha, V. V. Fluorescent Biosensors for Neurotransmission and Neuromodulation: Engineering and Applications. *Front. Cell. Neurosci.* **13**, (2019).

45. Xue, L. *et al.* Probing coenzyme A homeostasis with semisynthetic biosensors. *Nat. Chem. Biol.* **19**, 346–355 (2023).

46. Wang, W. *et al.* A Ratiometric Fluorescent Biosensor Reveals Dynamic Regulation of Long-Chain Fatty Acyl-CoA Esters Metabolism. *Angew. Chem. Int. Ed.* **60**, 13996–14004 (2021).

47. Du, Y., Hu, H., Pei, X., Du, K. & Wei, T. Genetically Encoded FapR-NLuc as a Biosensor to Determine Malonyl-CoA in Situ at Subcellular Scales. *Bioconjug. Chem.* **30**, 826–832 (2019).

48. Lieberman, W. K. *et al.* Chemoproteomics Yields a Selective Molecular Host for Acetyl-CoA. *J. Am. Chem. Soc.* **145**, 16899–16905 (2023).

49. Monteiro, D. C. F. *et al.* Formation of a heterooctameric complex between aspartate α-decarboxylase and its cognate activating factor, PanZ, is CoA-dependent. *Biochem. Biophys. Res. Commun.* **426**, 350–355 (2012).

50. Monteiro, D. C. F. *et al.* The structure of the PanD/PanZ protein complex reveals negative feedback regulation of pantothenate biosynthesis by coenzyme A. *Chem. Biol.* **22**, 492–503 (2015).

51. Stuecker, T. N., Tucker, A. C. & Escalante-Semerena, J. C. PanM, an acetyl-coenzyme A sensor required for maturation of L-aspartate decarboxylase (PanD). *mBio* **3**, e00158-12 (2012).

52. Lobas, M. A. *et al.* A genetically encoded single-wavelength sensor for imaging cytosolic and cell surface ATP. *Nat. Commun.* **10**, 711 (2019).

53. Zhang, C. & Ye, B.-C. A single fluorescent protein-based sensor for in vivo 2-oxogluatarate detection in cell. *Biosens. Bioelectron.* **54**, 15–19 (2014).

54. Roberts, T. M. *et al.* Identification and Characterisation of a pH-stable GFP. *Sci. Rep.* **6**, 28166 (2016).

55. Kostyuk, A. I., Demidovich, A. D., Kotova, D. A., Belousov, V. V. & Bilan, D. S. Circularly Permuted Fluorescent Protein-Based Indicators: History, Principles, and Classification. *Int. J. Mol. Sci.* **20**, 4200 (2019).

56. Jõers, A. & Tenson, T. Growth resumption from stationary phase reveals memory in Escherichia coli cultures. *Sci. Rep.* **6**, 24055 (2016).

57. Bren, A. *et al.* Glucose becomes one of the worst carbon sources for E.coli on poor nitrogen sources due to suboptimal levels of cAMP. *Sci. Rep.* **6**, (2016).

58. Martínez-Gómez, K. *et al.* New insights into Escherichia coli metabolism: carbon scavenging, acetate metabolism and carbon recycling responses during growth on glycerol. *Microb. Cell Factories* **11**, 46 (2012).

59. Chen, W. W., Freinkman, E., Wang, T., Birsoy, K. & Sabatini, D. M. Absolute quantification of matrix metabolites reveals the dynamics of mitochondrial metabolism. *Cell* **166**, 1324 (2016).

60. Takamura, Y. & Nomura, G. Changes in the Intracellular Concentration of Acetyl-CoA and Malonyl-CoA in Relation to the Carbon and Energy Metabolism of Escherichia coli K12. *Microbiology* **134**, 2249–2253 (1988).

61. Zhao, S. *et al.* ATP-citrate lyase controls a glucose-to-acetate metabolic switch. *Cell Rep.* **17**, 1037–1052 (2016).

62. Wellen, K. E. *et al.* ATP-Citrate Lyase Links Cellular Metabolism to Histone Acetylation. *Science* **324**, 1076–1080 (2009).

63. Trefely, S., Lovell, C. D., Snyder, N. W. & Wellen, K. E. Compartmentalised acyl-CoA metabolism and roles in chromatin regulation. *Mol. Metab.* **38**, 100941 (2020).

64. Bulusu, V. *et al.* Acetate Recapturing by Nuclear Acetyl-CoA Synthetase 2 Prevents Loss of Histone Acetylation during Oxygen and Serum Limitation. *Cell Rep.* **18**, 647–658 (2017).

65. Li, X. *et al.* Nucleus-Translocated ACSS2 Promotes Gene Transcription for Lysosomal Biogenesis and Autophagy. *Mol. Cell* **66**, 684-697.e9 (2017).

66. Sivanand, S. *et al.* Nuclear Acetyl-CoA Production by ACLY Promotes Homologous Recombination. *Mol. Cell* **67**, 252–265 (2017).